Rectangular Orthogonal Digital Filter Banks Based on Extended Gaussian Functions

Jin, Wei; Zhong, Zhuqiang; Jiang, Shan; He, Jiaxiang; Chang, Da; Hong, Yanhua; Giddings, Roger; Jin, Xianqing; O'Sullivan, Maurice; Durrant, Tim; Trewem, J.; Mariani, G.; Tang, Jianming

Journal of Lightwave Technology

DOI:
10.1109/JLT.2022.3153589

E-pub ahead of print: 23/02/2022

Peer reviewed version

Rectangular Orthogonal Digital Filter Banks Based on Extended Gaussian Functions

W. Jin, Z. Q. Zhong*, S. Jiang, J. X. He, D. Chang, Y. H. Hong, R. P. Giddings, X. Q. Jin, M. O'Sullivan, T. Durrant, J. Trewern, G. Mariani, and J. M. Tang *Member, IEEE*

***Abstract*—Rectangular orthogonal digital filter banks (ODFBs) based on square-root-raised-cosine (SRRC) functions are widely utilised to realise flexible and elastic multi-channel aggregations for fixed and mobile networks. However, long digital filter lengths are required to minimize digital filtering-associated signal distortions. In this paper, based on the extended Gaussian function (EGF), a novel rectangular ODFB with excellent robustness against the short digital filter length-induced truncation effect is proposed. Optimum digital filter parameters of the EGF-based ODFBs are identified and verified in multi-channel hybrid OFDM-digital filter multiple access (DFMA) PONs based on intensity modulation and direct detection (IMDD). By making use of the identified optimum digital filter parameters, extensive comparisons of digital filter characteristics and corresponding multi-channel upstream PON performances are made between the EGF-based ODFBs and the SRRC-based ODFBs. It is shown that to achieve a similar aggregated upstream signal transmission capacity, the EGF-based ODFB reduces the digital filter DSP complexity by a factor of 4. For a digital filter length as short as 8, in comparison with the SRRC-based ODFB, the EGF-based ODFB introduces >1.5dB (>0.8dB) improvements in upstream receiver sensitivity for 5-bits (8-bits) DACs/ADCs, increases the aggregated upstream signal transmission capacity by >5.5%, enlarges the ONU launch power dynamic range by >2.5dB and improves the frequency offset tolerance by a factor of >1.5. In addition, the EGF-based ODFB also enhances upstream performance robustness against ONU symbol timing offsets.**

***Index Terms*—filter bank, multi-channel aggregation, extended Gaussian function (EGF), square-root raised-cosine (SRRC).**

I. Introduction

As a key element of digital signal processing (DSP) techniques, digital filtering has been widely implemented in fixed and mobile networks to provide a large diversity of network functionalities including adaptive equalization [1], [2], pulse shaping [3], [4], multiple channel multiplexing and demultiplexing [5], [6]. For the fixed networks of the 5th generation and beyond [7], to effectively accommodate a large diversity of new use cases with diversified requirements on bandwidth, latency, coverage, QoS and security, it is envisaged that digital filtering acts as a promising physical layer technology to provide the fixed networks with sufficient flexibility, elasticity and adaptability. On the other hand, for the rollout of 5G and beyond mobile networks, advanced digital filtering techniques are also highly desirable for not only realizing the adaptive spectral confinement of waveforms transmitted over the radio/fiber links [8], [9], but also enabling the fronthaul mobile networks to provide, in a cost effective manner, dynamically reconfigurable, on-demand 'just-the-right-size' elastic connections each tailored to a specific application and/or service requirement [10], [11]. Such operations are vital for achieving the seamless convergence of separately developed and operated optical networks and mobile networks [12], [13]. Rectangular orthogonal digital filter banks (ODFBs) play an important role in cost-effectively equipping the fixed and mobile networks with the abovementioned salient DSP features [14]-[16].

From the multi-channel aggregation point of view, the rectangular ODFB-enabled multi-channel aggregation is inherently transparent to various network design characteristics [12], including signal modulation formats [12], [17], optical signal modulation and detection schemes (intensity modulation and direct detection-IMDD [15], [16] or coherent [18], [19]), network topologies and wavelength division multiplexing grids [20], [21]. It also has excellent compatibility with various existing multiplexing techniques including, for example, polarization multiplexing [22] and non-orthogonal multiplexing [13]. Moreover, due to the digital filtering operation, the out-of-band radiation of each channel can be effectively reduced without requiring extra electrical and/or optical analogue components. This offers reduced channel interferences, improved spectral efficiency and system cost effectiveness [16]. The rectangular ODFB-based passive optical networks (PONs) can be regarded as frequency division multiplexing (FDM) PONs. As such, the rectangular ODFB-based PONs can effectively address the high latency and latency jitter issues associated with time division multiplexing (TDM) PONs [23].

From the digital filter design point of view, a rectangular ODFB contains multiple orthogonal digital filter pairs, which is produced using sine and cosine modulations of a rectangular prototype filter [12], [14]. Such sine and cosine modulated digital filter banks are easy to be implemented because the

This work was supported in part by the DESTINI project funded by the ERDF under the SMARTExpertise scheme, and in part by the DSP Centre funded by the ERDF through the Welsh Government.

W. Jin, Z. Q. Zhong, S. Jiang, J. X. He, D. Chang, Y. H. Hong, R. P. Giddings, X. Q. Jin and J. M. Tang are with the School of Computer Science and Electronic Engineering, Bangor University, Bangor, LL57 1UT, UK. (email: z.zhong@bangor.ac.uk; w.jin@bangor.ac.uk; j.tang@bangor.ac.uk).

M. O'Sullivan is with Ciena Canada, Inc., 385 Terry Fox Drive, Ottawa, Ontario K2K 0L1, Canada.

T. Durrant and J. Trewern are with EFFECT Photonics LTD., Brixham Laboratory, Freshwater Quarry, Brixham, Devon, England, TQ5 8BA, UK.

G. Mariani is with EFFECT Photonics B.V., Kastanjelaan 400, 5617BC Eindhoven, Netherlands.

overall DSP computational complexity and subsequent cost are determined mainly by the prototype filter and modulation [24]. For each individual orthogonal digital filter pair, their frequency responses have a similar amplitude profile but a π/2 phase difference. In IMDD transmission systems, each orthogonal digital filter pair can be used for independently conveying two signals sharing the same radio frequency spectral region, here termed sub-wavelength throughout this paper. In comparison with the cosine-modulated digital filter banks capable of only transmitting a single real-valued signal in each individual sub-wavelength [25], [26], the rectangular ODFBs can convey complex-valued signals, thus they are transparency to signal modulation formats and improve the spectral efficiency. On the other hand, for transmission systems utilising offset quadrature amplitude modulation (OQAM), including, for example, filter-bank multicarrier/OQAM (FBMC/OQAM) systems [27]-[29] and OQAM carrier-less amplitude and phase modulation (OQAM-CAP) systems [30], in comparison with the rectangular prototype filters, the non-rectangular prototype filters can just achieve a high spectral efficiency and/or low computational complexity [29], [30]. However, they cannot be used to produce the highly desirable ODFBs, because the resulting ODFBs with the non-rectangular frequency responses give rise to severe channel interferences and limited performance transparency to signal modulation formats. In addition, filtered-orthogonal frequency division multiplexing (filtered-OFDM) has been adopted in the 3rd Generation Partnership Project (3GPP)-released 5G waveform technical specifications [31]. In conventional filtered-OFDM systems [31], [32], the rectangular prototype filter designs are widely based on the soft truncation of a windowed Sinc function [31]. The window functions play a vital role in determining the resulting digital filter characteristics. However, in the filtered-OFDM systems, the rectangular digital filter banks are produced by simply allocating the prototype filters at the desired frequencies of a specific spectral region, the resulting digital filter banks are thus complex-valued and offer the least compatibility with the cost-effective IMDD transmission systems compared to the real-valued rectangular ODFBs.

In all previously published work [5], [6], [10]-[22], [25], [26], to the best knowledge of the authors, the rectangular ODFBs are produced using a prototype filter having a square-root-raised-cosine (SRRC) profile only. To minimise signal distortions due to imperfect digital filter implementation, the SRRC-based ODFBs have to use a sufficiently long digital filter length to achieve desirable digital filter characteristics, i.e., flat passbands, sharp transition bands and sufficiently large stopband attenuations. However, since a long digital filter length unavoidably leads to a high digital filter DSP complexity, therefore, it is beneficial if an advanced ODFB with a short digital filter length is made available, which can still offer excellent robustness against the short filter length-induced truncation effect.

To address the abovementioned challenge, this paper reports a novel rectangular ODFB based on extended Gaussian function (EGF) [24], [33]. The conventional EGF prototype filter has a non-rectangular frequency response profile and thus cannot be directly used to construct the highly desirable rectangular ODFBs. In this paper, to enable the EGF-based ODFB to have a rectangular frequency response profile, the optimum digital filter parameters of the proposed ODFB are identified numerically in an upstream orthogonal digital filtering based OFDM multi-channel IMDD PON. Based on the identified optimum digital filter parameters, the salient features of the proposed ODFBs are extensively explored through comprehensive comparisons of digital filter characteristics and multi-channel transmission performances between the EGF-based ODFB and the conventional SRRC-based ODFB. In comparison with the conventional SRRC-based ODFB, the EGF-based ODFB has the following three unique features:

1. Enhanced robustness against the short digital filer length-induced truncation effect. For digital filter lengths of L⩾32, the proposed ODFB has almost similar digital filter frequency responses. For the considered PON, for digital filter lengths varying from L=8 to L=256, the upstream transmission performances and aggregated upstream signal transmission capacity are almost independent of digital filter length.
2. Improved signal transmission performances and performance robustness to differential ONU launch power variations and ONU symbol timing/frequency offsets for a digital filter length as short as L=8.
3. Considerably reduced digital filter DSP complexity. To deliver an aggregated upstream signal transmission capacity similar to that supported by the proposed ODFB with a digital filter length of L=8, the SRRC-based ODFB must use a digital filter length of ⩾32.

II. Orthogonal Digital Filter Banks

A. EGF-based ODFB Design

In an ODFB, each orthogonal digital filter pair contain an in-phase (I-phase) digital filter and a quadrature-phase (Q-phase) digital filter [14]. The impulse responses of the orthogonal digital filter pair can be expressed as,

$$\begin{cases} h_{i-I}(t) = z_{\alpha,\nu,\tau}(t)\cos(2\pi f_{ci}t) \\ h_{i-Q}(t) = z_{\alpha,\nu,\tau}(t)\sin(2\pi f_{ci}t) \end{cases} \quad (1)$$

where $h_{i\text{-}I}(t)$ and $h_{i\text{-}Q}(t)$ are the impulse responses of the i-th orthogonal digital filter pair with the subscript I and Q presenting the I-phase and Q-phase digital filters respectively. f_{ci} stands for the central frequency of the i-th orthogonal digital filter pair. $z_{\alpha,\nu,\tau}(t)$ is the EGF with a closed-form expression given by [24], [33],

$$z_{\alpha,\nu,\tau}(t) = \frac{1}{2}\left\{\sum_{k=0}^{\infty} d_{k,\alpha,\nu}\left[g_\alpha\left(t'+\frac{k}{\nu}\right)+g_\alpha\left(t'-\frac{k}{\nu}\right)\right]\right\} \times \sum_{l=0}^{\infty} d_{l,\frac{1}{\alpha},\tau}\cos\left(2\pi l\frac{t'}{\tau}\right),\ t'=\frac{t}{T} \quad (2)$$

where T is the symbol period and $g_\alpha(t)$ represents the Gaussian function expressed as,

$$g_\alpha(t) = (2\alpha)^{\frac{1}{4}}e^{-\pi\alpha t^2},\ \alpha>0 \quad (3)$$

with α being the spreading parameter. In Eq. (2), the real-valued coefficients of $d_{k,\alpha,v}$ is given by [24],

$$d_{k,\alpha,v} = \sum_{l=0}^{\infty} a_{k,l} e^{\frac{-\alpha\pi l}{2v^2}} \approx \sum_{r=0}^{n} b_{k,r} e^{\frac{-\alpha\pi}{2v^2}(2r+k)}, \ 0 \le k \le K \quad (4)$$

where n is the positive integer satisfying $n=\lfloor (K-k)/2 \rfloor$, here $\lfloor \cdot \rfloor$ denotes the operation of rounding to the nearest inferior integer. K is the positive integer used to appropriately truncate the infinite summation in Eq. (4), and we take K=14 in this paper. A table of typical $b_{k,r}$ coefficients corresponding to K=14 can be found in [24].

The digital filter length, L, is defined as the number of original data samples simultaneously contributing to the filtering process at digital filter input [17].

B. *Orthogonal Digital Filter Characteristic Comparisons*

For the proposed ODFBs based on EGF, their optimum digital filter parameters are {α=0.23, ν=0.9, τ=1}, which are numerically identified in Section III. For different digital filter lengths, the frequency responses of an orthogonal digital filter pair based on EGF and SRRC are plotted in Fig. 1. In this paper, the SRRC roll-off coefficient of 0.1 is considered. It can be found from Fig. 1 that for the EGF-based orthogonal digital filters, prolonging the digital filter length from L=4 to L=16 increases the digital filter stopband attenuations. While when digital filter lengths are ≥32, the digital filter length variations do not introduce obvious changes in the digital filter frequency responses. On the other hand, for the SRRC-based orthogonal digital filters, different digital filter lengths give rise to considerable differences in the digital filter frequency responses, especially in the filter stopband attenuations.

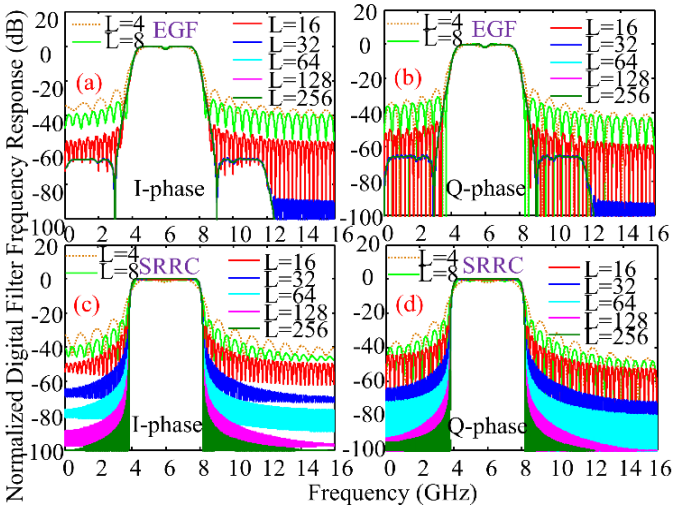

Fig. 1 Normalized frequency responses of an orthogonal digital filter pair for different digital filter lengths. (a) I-phase digital filters based on EGF; (b) Q-phase digital filters based on EGF; (c) I-phase digital filters based on SRRC; (d) Q-phase digital filters based on SRRC.

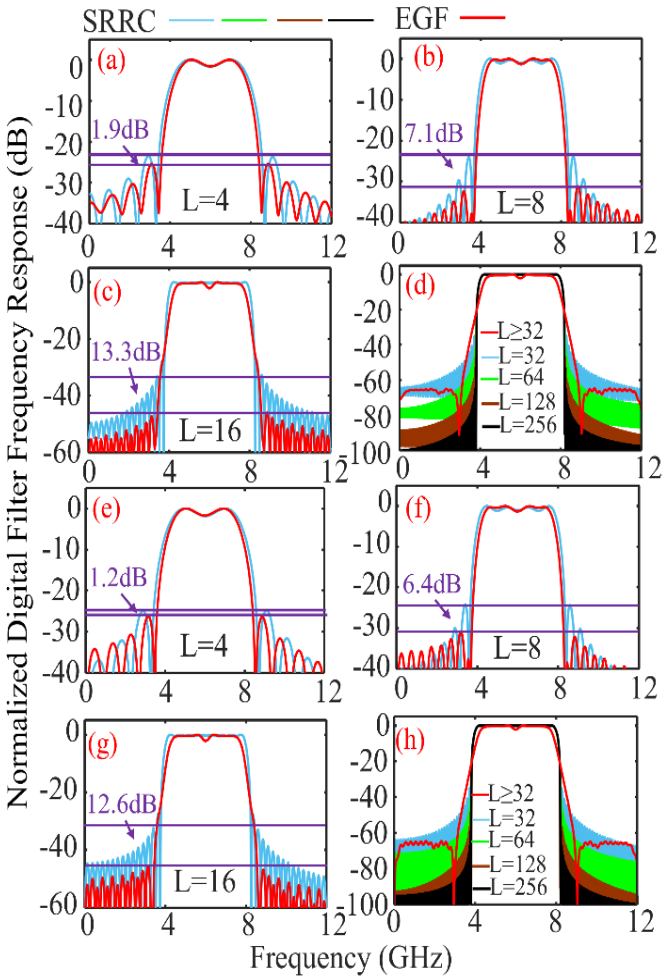

Fig. 2 Stopband characteristics of an orthogonal digital filter pair for different digital filter lengths. (a)~(d) I-phase digital filters; (e)~(h) Q-phase digital filters.

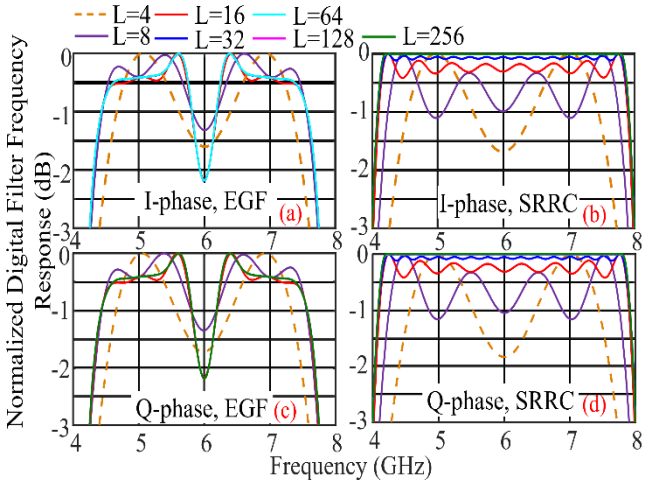

Fig. 3 Passband characteristics of an orthogonal digital filter pair for different digital filter lengths. (a) I-phase digital filters based on EGF; (b) I-phase digital filters based on SRRC; (c) Q-phase digital filters based on EGF; (d) Q-phase digital filters based on SRRC.

For different digital filter lengths, the stopband attenuations of the EGF and SRRC-based orthogonal digital filters are compared in detail in Fig. 2. It can be found that for digital filter lengths of L=4, the EGF and SRRC-based orthogonal digital

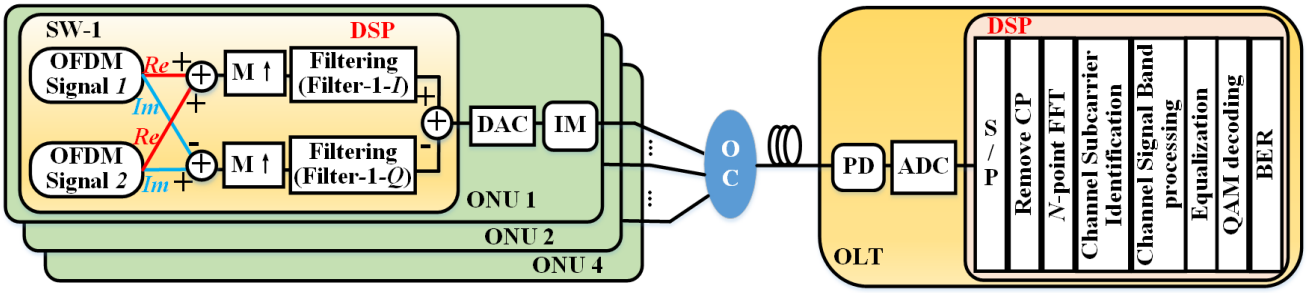

Fig. 4 Simulation setup of an upstream orthogonal digital filtering enabled OFDM multi-channel IMDD PON with 4 ONUs. M↑: digital up-sampling by a factor of M, SW: sub-wavelength, Re/Im: real/imaginary part, OC: optical coupler.

filters have similar stopband attenuations and passband ripples. While for digital filter lengths of L=8 (L=16), the EGF-based I-phase/Q-phase digital filters have ~7.1dB/~6.4dB (~13.3dB/~12.6dB) increases in the stopband attenuations. When the digital filter lengths are further increased to ≥64, the SRRC-based orthogonal digital filters have relatively large stopband attenuations in comparison with the EGF-based orthogonal digital filters. In addition, for the SRRC-based orthogonal digital filters, a long digital filter length gives rise to a large stopband attenuation, this agrees well with the results presented in [17]. However, for digital filter lengths of L⩾32, the EGF-based orthogonal digital filters have similar stopband characteristics compared to the SRRC counterparts.

The passband ripples of the EGF and SRRC-based orthogonal digital filters are illustrated in Fig. 3. For the SRRC-based orthogonal digital filters, a long digital filter length results in a relatively flat top, this agrees well with the results reported in [17]. For the EGF-based orthogonal digital filters with the identified optimum digital filter parameters, the passband ripples mainly occur at the central frequencies of the digital filters. It is also interesting to find that for digital filter lengths of L≥16, the EGF-based orthogonal digital filters have similar passband characteristics and the central frequency ripples are approximately 2.3dB. While for a digital filter length of L=8, the passband central frequency ripples of the EGF-based orthogonal digital filters are reduced to ~1.3dB, but the ripple-affected spectral regions are slightly broadened.

From the digital filter frequency response characteristics discussed above, we can see that in comparison with the SRRC-based ODFBs, the proposed ODFBs based on EGF have the following features: 1) for digital filter lengths of L≥32, the digital filter frequency responses are similar, 2) for digital filter lengths of L=8 (L=16), the EGF-based ODFBs have at least ~6.4dB (~12.6dB) increases in the stopband attenuations, and 3) the passband ripples are ~1.3dB (~2.3dB) for digital filter lengths of L=8 (L≥16) and the ripples are mainly located at the digital filter central frequencies.

III. System Setup and Optimum Digital Filter Parameter Identification

In this section, a multipoint-to-point upstream orthogonal digital filtering enabled OFDM multi-channel IMDD PON, termed hybrid single sideband (SSB) OFDM-digital filter multiple access (DFMA) PON [14]-[16], is utilized to identify the optimum digital filter parameters of the proposed ODFBs.

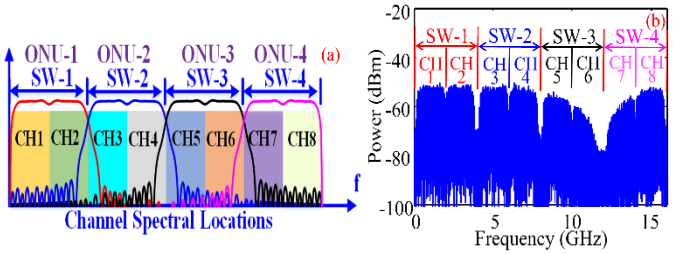

Fig. 5 (a) Channel spectral locations and (b) signal spectrum after 30km SSMF transmissions. CH6 and CH7 are not operational due to the chromatic dispersion-induced channel fading effects. SW: sub-wavelength.

Table 1

Parameter	Value
IFFT/FFT size	32/256
Data-bearing subcarriers	14
Up-sampling factor (M)	8
Modulation formats	16-QAM
Cyclic prefix ratio	1/16
Clipping ratio	9dB
SRRC roll-off coefficient	0.1
DAC/ADC sampling speed	32GS/s
DAC/ADC resolution	8-bit
SSMF fiber length	30km
Fiber Dispersion	16 ps/nm/km
PIN detector quantum efficiency	0.8
PIN detector Sensitivity	-19dBm

A. System Setup

The upstream PON network architecture considered in numerical simulations is presented in Fig. 4. It contains four optical network units (ONUs) each producing two independent SSB OFDM signals and utilizing an orthogonal digital filter pair to locate these two independent SSB OFDM signals at the desired sub-wavelength spectral region. The channel spectral locations of the produced eight SSB OFDM signals are presented in Fig. 5. To produce these SSB OFDM signals, a complex-valued OFDM signal modulation operation [14] is applied, where half of the subcarriers within a signal band are set at zeros. Therefore, each complex OFDM signal is a SSB signal, and its real part and (-1)-multiplied imaginary part form a Hilbert transform pair. In generating these OFDM signals, the adopted key parameters are listed in Table 1. As seen in Fig. 4, in each ONU, the two complex SSB OFDM signals first undergo a digital up-sampling operation (M↑) and then are digitally filtered using a specific orthogonal digital filter pair.

To support 8 SSB OFDM channels, a digital up-sampling factor of M=8 is employed here. The digital filter length is taken to be L=16. The resulting EGF-based I-phase and Q-phase digital filters thus have similar frequency responses, and the frequency responses of the Q-phase digital filters are plotted in Fig. 5(a). An 8-bit resolution at a sampling speed of 32GS/s is used for digital-to-analog converters (DACs) and analog-to-digital converters (ADCs). The adopted electrical signal clipping level is 9dB. The bitrate of each SSB OFDM signal is 6.58Gbit/s, this gives rise to an aggregated upstream raw signal bit rate of 52.7Gbit/s. Similar to the conditions reported in [14], ideal intensity modulation is considered in each ONU, and after combining the optical signals from these 4 ONUs, the overall optical launch power into the PON is fixed at 6dBm.

After 30km standard single mode fiber (SSMF) transmissions, in the optical line terminal (OLT), an optical-electrical (O-E) conversion is performed, and then a FFT operation-based DSP operation is used for signal demultiplexing and demodulation. As seen in Fig. 4, in the OLT DSP, a deserializer converts the serial sample stream emerging from an ADC to 272 parallel sample streams, which corresponds in length to one symbol period. After removing cyclic prefix (CP) with 16 samples in length, a 256-point FFT operation is then performed to demultiplex and demodulate all the SSB OFDM signals. At the output of the FFT, the 128 subcarriers at the positive frequency bins are evenly classified into 8 subcarrier groups. Each subcarrier group contains 16 subcarriers and corresponds to a SSB OFDM signal. In the subsequent channel signal processing operation, a conjugation operation and a subcarrier reverse ordering operation are performed for the SSB OFDM signals locating at the low frequency region of their occupied sub-wavelengths, and as seen in Fig. 5(a), these channels include CH1, CH3, CH5, and CH7. While the remaining channels (CH2, CH4, CH6, and CH8) do not require such operations. After the conventional OFDM subcarrier equalizations, QAM decoding is performed for the data-bearing subcarriers for each channel.

The above simulation setup and parameters are used to explore the optimum parameters set of {α, ν, τ} of the proposed ODFBs. For the orthogonal digital filter pairs embedded in different ONUs, the impacts of the digital filter parameter variations on digital filter frequency responses are similar, and for each orthogonal digital filter pair, the I-phase and Q-phase digital filters have similar frequency responses. Therefore, in the following sections, only the ONU-2-embedded I-phase digital filter' frequency responses are given to demonstrate the impacts of the digital filter parameter variations on their frequency responses.

B. Optimum α Parameter for ODFBs Based on EGF

The α parameter determines the decay of the EGF prototype filters in the time domain and the stopband attenuations of the resulting ODFBs in the frequency domain.

To identify the optimum α parameter of the proposed ODFBs, the digital filter parameter set of {ν=0.9, τ=1} are used. For different α parameters, the impulse responses of the baseband EGF prototype filters and the frequency responses of the resulting ONU-2-embedded I-phase digital filters are illustrated in Fig. 6(a) and Fig. 6(b), respectively. It can be found that the α parameter determines the decay of the EGF prototype filters in the time domain and the stopband attenuations of the resulting ODFBs in the frequency domain. The impulse responses of the EGF prototype filters decay fast with increasing the α parameter. However, for the EGF-based ODFBs with α≥0.4, increasing α results in relatively small digital filter stopband attenuations. As seen in Fig. 6(b), α>0.1 is also necessary for achieving a flat top. As such, the optimum α falls into the range of 0.1<α<0.4.

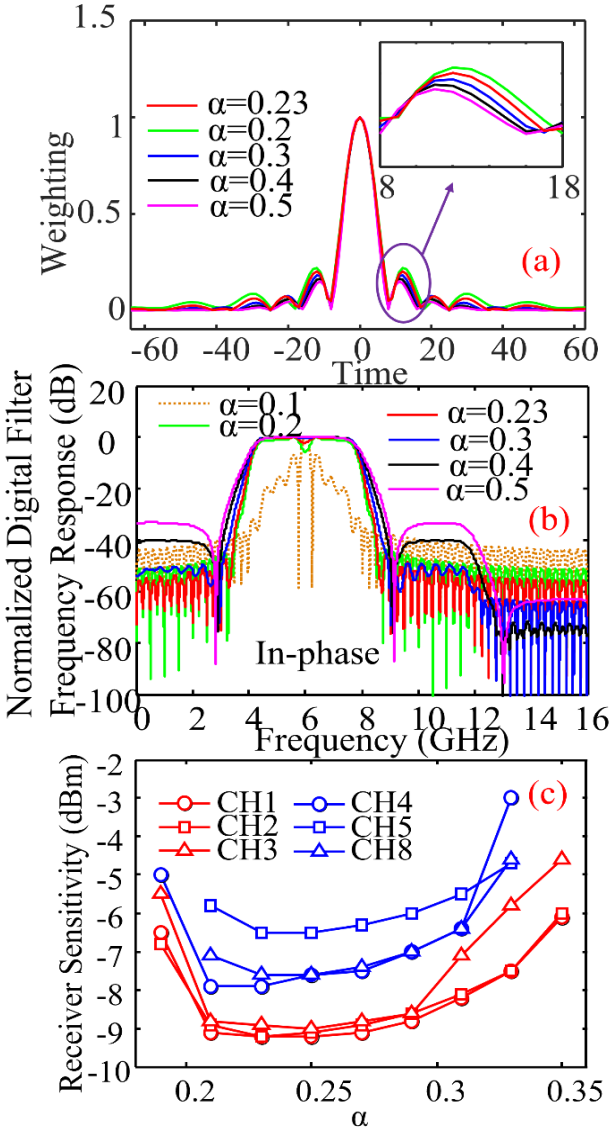

Fig. 6 Impacts of α parameters on (a) impulse response of baseband EGF prototype filters, (b) frequency responses of ODFBs based on EGF, and (c) upstream transmission performances.

For the considered PONs, the impacts of α parameter variations on the upstream transmission performances are explored and the results are illustrated in Fig. 6(c), where for each channel, the minimum received optical power at the OLT to achieve a bit error rate (BER) at the forward error correction (FEC) limit of 1×10^{-3} (defined as receiver sensitivity) is demonstrated. As shown in Fig. 5(b), CH6 and CH7 are not

operational due to the chromatic dispersion-induced channel fading effect and therefore, their transmission performances are not shown in Fig. 6(c). Fig. 6(c) shows that the optimum α parameter is ~0.23, and that an α parameter variation from 0.21 to 0.29 just introduces a receiver sensitivity degradation as low as <1dB.

C. *Optimum ν Parameter for ODFBs Based on EGF*

The ν parameter determines the main lobe widths of the impulse responses of the EGF prototype filters and the filter passband and transition region bandwidths of the resulting ODFB frequency responses.

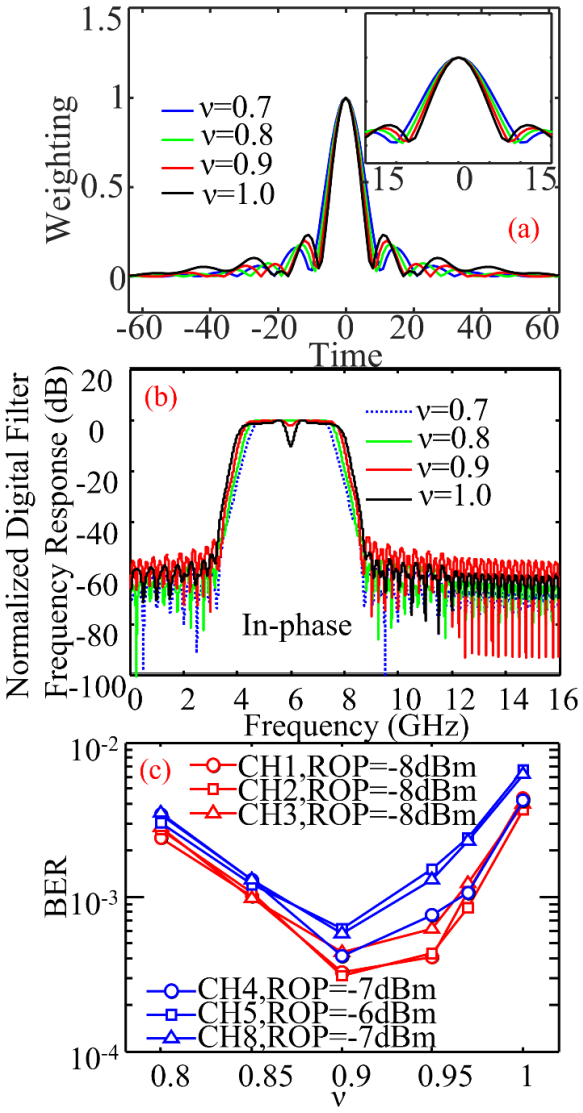

Fig. 7 Impacts of ν parameters on (a) impulse response of baseband EGF prototype filters, (b) frequency responses of ODFBs based on EGF, and (c) upstream transmission performances.

Here the digital filter parameter set of {α=0.23, τ=1} are used to identify the optimum ν parameter of the proposed ODFBs. With different ν parameters, the impulse responses of the baseband EGF prototype filters and the frequency responses of the resulting ONU-2-embedded I-phase digital filters are shown in Fig. 7(a) and Fig. 7(b), respectively. It can be found that a large ν parameter results in a narrow main lobe of the impulse responses of the EGF prototype filters. The resulting ODFBs thus have relatively wide filter passbands and narrow filter transition regions. For the rectangular ODFBs, a steep filter transition region is desirable. However, for ν≥0.9, a power dip occurs at the central frequency of the digital filter passband. In the considered PONs, for different ν parameters, the BER performances of the six operational channels at the specific received optical powers are demonstrated in Fig. 7(c). For each channel, a specific received optical power is selected, which is close to its receiver sensitivity as shown in Fig. 11(a). The results indicate that the optimum ν parameter is ~0.9.

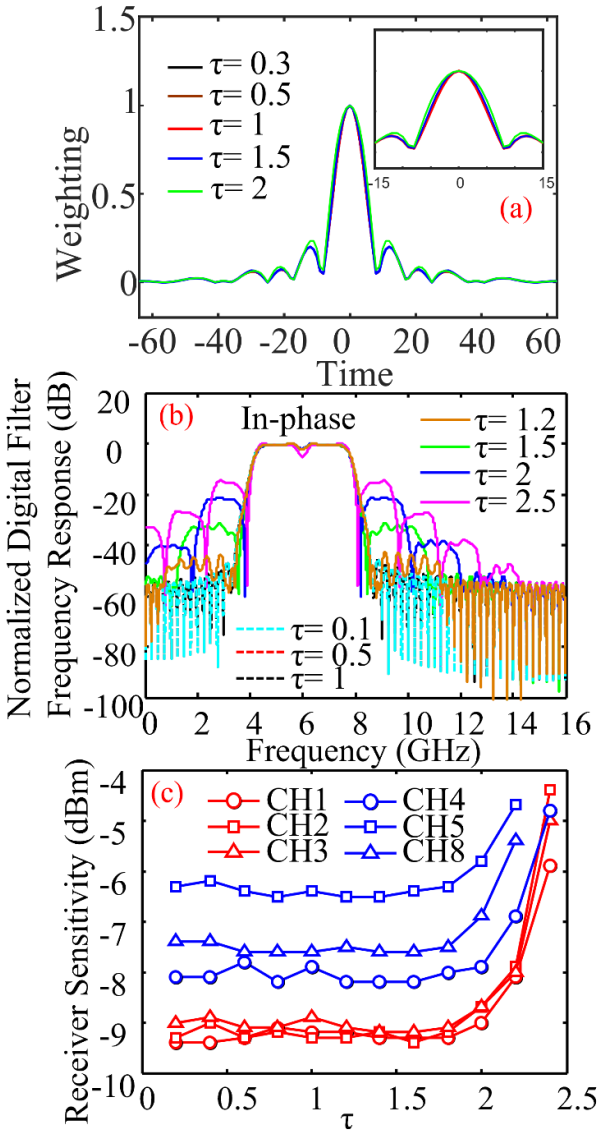

Fig. 8 Impacts of τ parameters on (a) impulse response of baseband EGF prototype filters, (b) frequency responses of ODFBs based on EGF, and (c) upstream transmission performances.

D. *Optimum τ Parameter for ODFBs Based on EGF*

When the τ parameter is <1.2, the variations of the τ parameter have no obvious influence on the digital filter impulse responses and frequency responses of the EGF prototype filters and the resulting ODFBs.

The impacts of the τ parameters on the impulse responses of the baseband EGF prototype filters, the frequency responses of the resulting ONU-2 embedded I-phase digital filters and the corresponding receiver sensitivities of the six operational channels in the considered PONs are shown in Fig. 8(a), Fig. 8(b), and Fig. 8(c), respectively. In obtaining these figures, the digital filter parameter set of {α=0.23, ν=0.9} are utilized. In Fig. 8(a), for τ≤1, the baseband EGF prototype filters have similar digital filter impulse responses, similar digital filter frequency responses are therefore observed for the resulting ODFBs, as seen in Fig. 8(b). As such, no significant changes can be found in the upstream transmission performances of the six operational channels when increasing τ from 0.2 to 1. However, when τ is >1.2, as seen in Fig. 8(b), the resulting ODFB stopband attenuations are reduced. In particular, significant reductions in the stopband attenuations occur for τ>1.5. Such reductions in the filter stopband attenuation unavoidably introduce considerable channel interferences. As a direct result, the upstream signal transmission performances of the six operational channels are degraded, as seen in Fig. 8(c). For practical implementation, the optimum τ parameter is thus taken to be 1 to simplify the digital filter implementation complexity.

IV. Upstream PON Transmission Performances

In this section, utilizing the EGF-based ODFBs with the identified optimum digital filter parameter set of {α=0.23, ν=0.9, τ=1}, the upstream transmission performances of the hybrid SSB OFDM-DFMA PONs are explored, by taking into account the simulation setup and parameters presented in Section III. Comprehensive performance comparisons are made between the proposed ODFB and the SRRC-based ODFB. The purpose of this excises is to identify the unique features associated with the proposed ODFBs.

A. Optimum Clipping Radio

Insufficient OFDM signal clipping leaves the signal with a high peak to average power ratio (PAPR), which further gives rise to an increase in the DAC/ADC quantization noise effect. To achieve the best upstream PON transmission performance, the optimum clipping ratio is identified in a back-to-back (B2B) optical system. The results are depicted in Fig. 9, in which for simplicity, the obtained CH2 BER contours are plotted against clipping radio and DAC/ADC quantization bit. A digital filter length of L=8 and a received optical power of -8dBm are adopted. It can be found in Fig. 9 that the PONs incorporating the EGF-based and SRRC-based ODFBs have a similar optimum clipping radio of ~9dB. This is because for these two ODFBs, their PAPRs of the digitally filtered OFDM signals are similar. This can be verified in Fig. 10, where the complementary cumulative distribution functions (CCDFs) of the digitally filtered CH2 OFDM signals with different digital filter lengths and modulation formats are presented. The variations in digital filter length and modulation format have no significant impacts on the PAPRs of the digitally filtered OFDM signals.

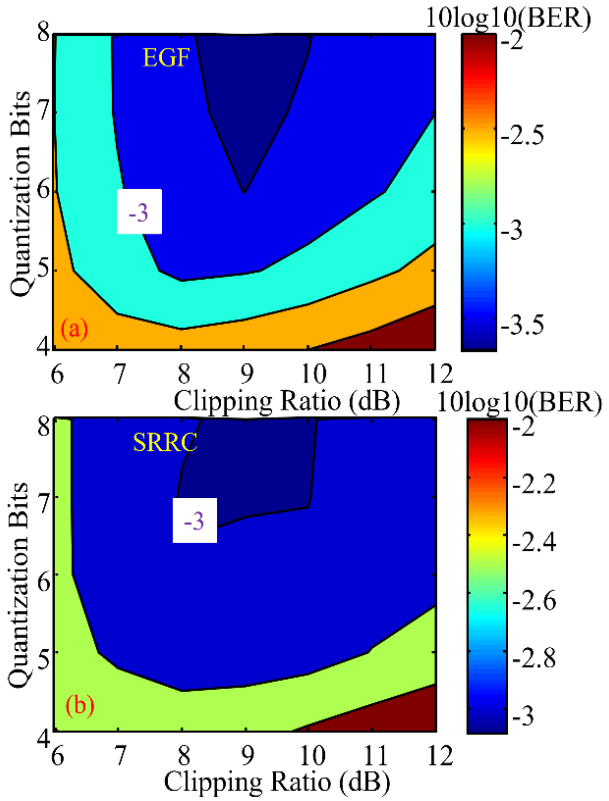

Fig. 9 BER contours against clipping radio and DAC/ADC quantization bits. (a) EGF-based ODFBs; (b) SRRC-based ODFBs.

B. Upstream PON Transmission Performances

Using the identified optimum clipping ratio of 9dB, the system setup and corresponding parameters presented in Section III(A), the upstream transmission performances of the PONs incorporating the EGF-based and SRRC-based ODFBs are explored. The numerically simulated results are presented in Fig. 11. The digital filter length is taken to be L=8. In comparison with the SRRC-based ODFBs, the proposed ODFBs give rise to >0.8dB receiver sensitivity improvements. This is because, for the considered digital filter length of L=8, the proposed ODFBs have ~6.4dB increases in the stopband attenuations, thus leading to reduced channel interferences. This is also verified by the results shown in Fig. 12(b), where the channel interference-induced power penalties are presented.

C. Impacts of Digital Filter Length on Upstream PON Transmission Performance

As seen in Fig. 1, for the ODFBs based on EGF and SRRC, the variations of digital filter length may result in different digital filter characteristics, and thus lead to different upstream PON transmission performances. By utilizing the simulation parameters in obtaining Fig. 11, the digital filter length variation-induced receiver sensitivity changes are shown in Fig. 12(a), which shows that for the EGF-based ODFBs, increasing digital filter length from L=8 to L=256 only alters the receiver sensitivity by <0.5dB. While for the SRRC-based ODFBs, the receiver sensitivity variations are as high as >2dB, and more importantly, a significant performance improvement occurs when the digital filter length is increased from L=8 to L=16. Therefore, the optimum digital filter length of the EGF-based

(SRRC-based) ODFBs is L=8 (L=16). In comparison with the SRRC-based ODFBs with their digital filter lengths of L⩾16, the proposed ODFB with a digital filter length of L=8 just degrade the receiver sensitivity by <1.3dB.

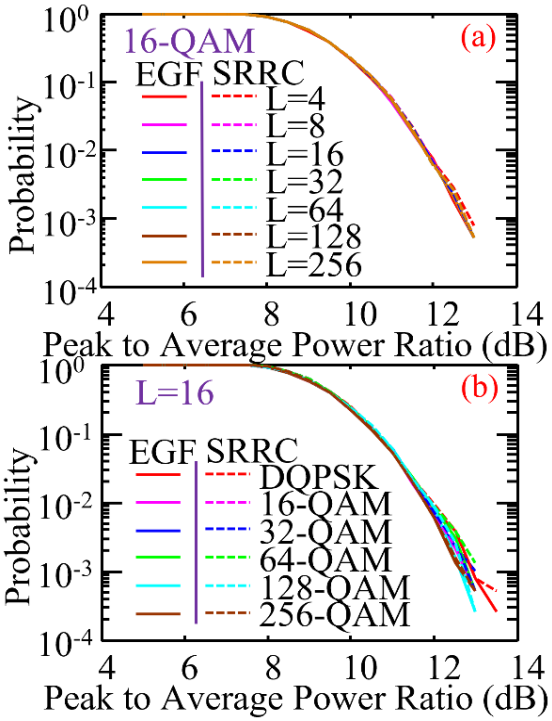

Fig. 10 CCDF curves of digitally filtered OFDM signals for (a) different digital filter lengths and (b) different modulation formats.

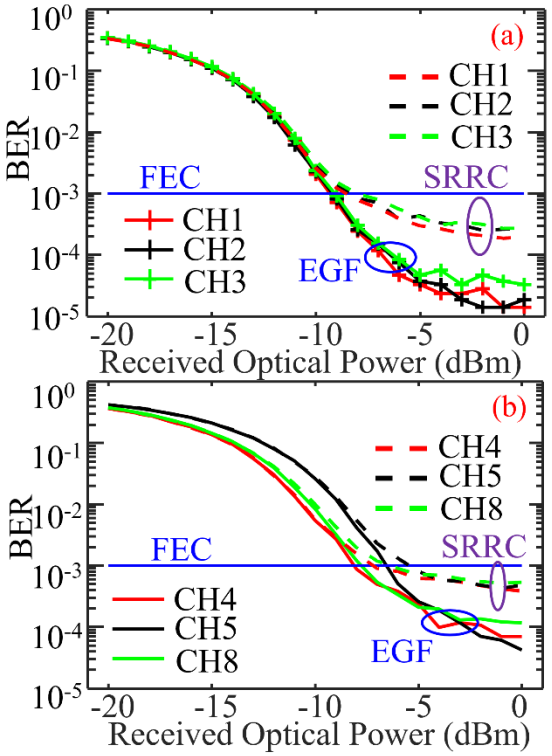

Fig. 11 Upstream transmission performances for (a) EGF-based ODFBs and (b) SRRC-based ODFBs.

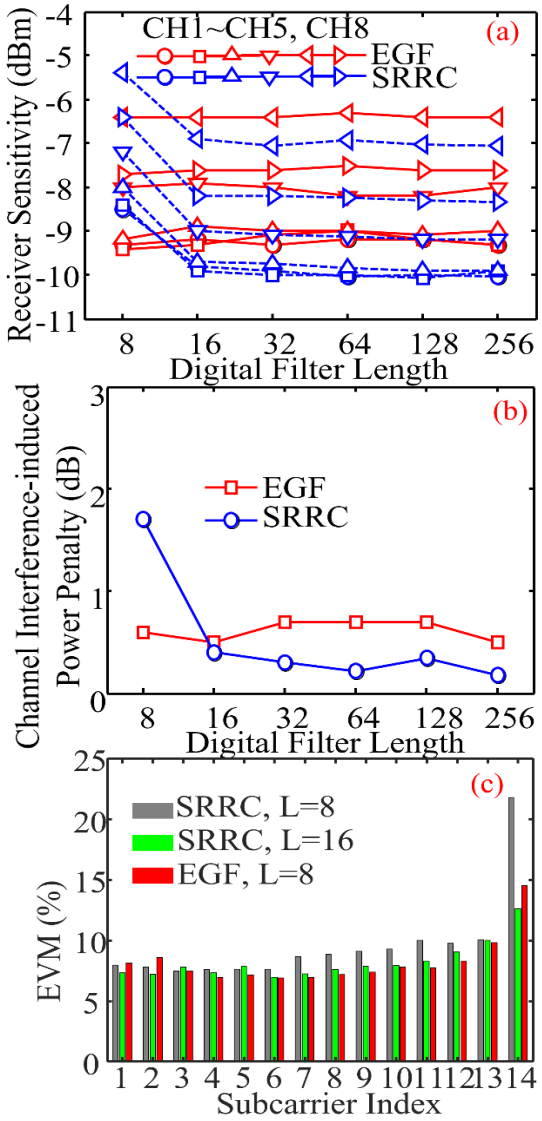

Fig. 12 Impacts of digital filter length variations on (a) receiver sensitivity and (b) channel interferences-induced power penalty. (c) Subcarrier EVM performances.

To gain an in-depth understanding of the influence of digital filter length on the upstream PON transmission performance, the power penalties arising from digital filter length-associated channel interferences are explored for different digital filter lengths. The power penalty is obtained by calculating the receiver sensitivity differences of a specific OFDM channel with and without a sub-wavelength-wide spectral space between itself and its adjacent channels. The results are presented in Fig. 12(b). For the EGF-based ODFBs with their digital filter lengths varying from L=8 to L=256, the channel interference-caused power penalties are similar. While for the SRRC-based ODFBs, when the digital filter lengths are <16, a relatively large channel interference occurs mainly because of the short digital filter length-induced reductions in the digital filter stopband attenuations, as seen in Fig. 1. When the digital filter lengths are ≥16, the SRRC-based orthogonal digital filters have sufficient stopband attenuations, thus leading to the reduced channel interference effect. This verifies, from a different angle, that the optimum digital filter lengths for the

EGF-based and SRRC-based ODFBs are L=8 and L=16 respectively.

Because the orthogonal digital filter pairs embedded in different ONUs have similar digital filter frequency responses, the OFDM signals in different channels thus suffer similar signal distortions associated with digital filtering. For a received optical power of -5dBm, the subcarrier error vector magnitude (EVM) performances of CH3 OFDM signal are presented in Fig. 12(c). For both the EGF-based and SRRC based ODFBs, the 14th subcarrier located in the vicinity of the digital filter transition band suffers from severe performance degradations due to the filter transition band-induced power reductions and the relatively large channel interferences. On the other hand, for the EGF-based ODFBs, the 1st and 2nd subcarriers located at the digital filter central frequency suffer from a filter central frequency power dip, thus slightly degraded EVM performances are observed. When the digital filter length is L=8, for the remaining subcarriers (3rd~13th), the EGF-based ODFBs have relatively better or similar EVM performances in comparison with the SRRC-based ODFBs. This is because for such a digital filter length, apart from the regions close to the digital filter central frequency and transition bands, the passband ripples of the EGF-based ODFBs are relatively small in comparison with the SRRC-based ODFBs, as seen in Fig. 3.

D. Impacts of DAC/ADC Resolution Bits on Upstream PON Transmission Performances

For a digital filter length of L=8, the impacts of the DAC/ADC resolution bit variations on receiver sensitivity are explored and the results are depicted in Fig. 13. In calculating this figure, except the DAC/ADC resolution bits, all other parameters are kept identical to those used in obtaining Fig. 11. For a DAC/ADC resolution bit as small as 5-bit (8-bit), the EGF-based ODFBs improve the receiver sensitivity by >1.5dB (>0.8dB) in comparison with the SRRC-based ODFBs. This implies that for such a digital filter length, the proposed EGF-based ODFBs outperform the SRRC-based ODFBs in terms of improving the PON upstream performance robustness against the DAC/ADC resolution bit reductions.

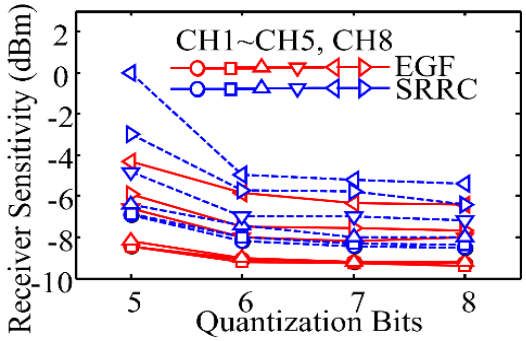

Fig. 13 Impacts of DAC/ADC resolution bit versions on receiver sensitivity.

E. Maximum Achievable Upstream PON Transmission Capacity

Using the system setup and parameters adopted in Fig. 11, for different digital filter lengths and SSMF transmission distances, the maximum achievable upstream signal transmission capacities for the EGF-based and SRRC-based ODFBs are calculated. Adaptive bit-loading is applied for each SSB OFDM signal with signal modulation formats varying from differential binary phase shift keying (DBPSK) to 64-QAM. As shown in Fig. 14(a), for the EGF-based ODFBs, similar aggregated upstream signal transmission capacities are observed for digital filter lengths of L≥8. For the SRRC-based ODFBs, the digital filter length variations from L=8 to L=32 increase the aggregated upstream signal transmission capacities, while when digital filter lengths are >32, no considerable aggregated upstream signal transmission capacity improvements are observed. When a digital filter length of L=8 is utilized, for different upstream transmission distances, the EGF-based orthogonal digital filter-induced aggregated upstream signal transmission capacity improvement ratios are presented in Fig. 14(b). In comparison with the SRRC-based ODFBs, the proposed ODFBs improve the aggregated upstream signal transmission capacity by >5.5% for a digital filter length of L=8.

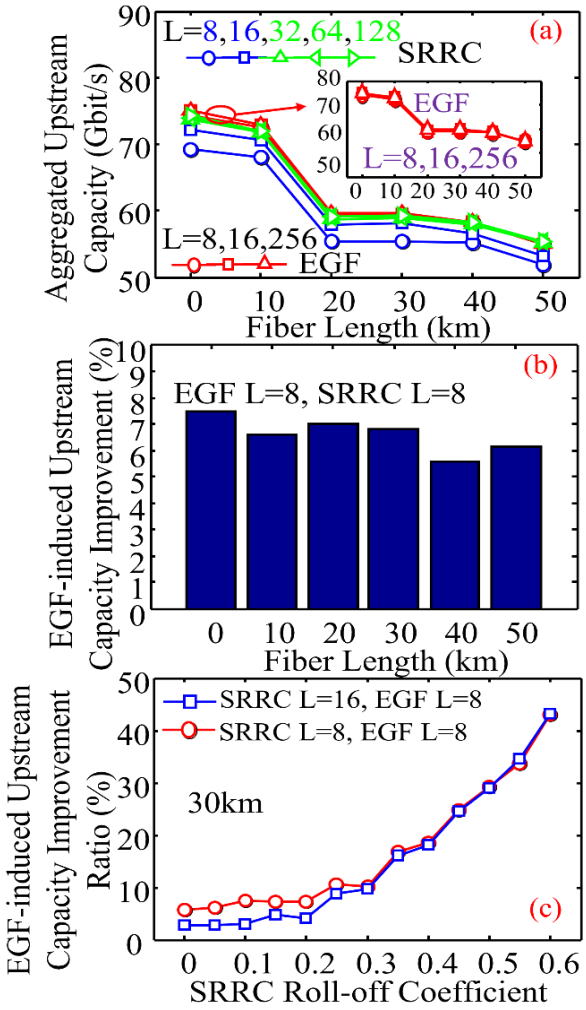

Fig. 14 (a) Maximum available aggregated upstream transmission capacity for different digital filter lengths and upstream transmission distances. EGF-based orthogonal digital filter induced aggregated upstream capacity improvement ratio for (b) a digital filter length of L=8 and (c) different SRRC roll-off coefficients. In (a) and (b), a SRRC roll-off coefficient of 0.1 is utilized.

In Fig. 14(a), it is also interesting to note that in comparison with the proposed ODFBs with a digital filter length of L=8, to achieve a similar aggregated upstream signal transmission

capacity, a minimum digital filter length of L=32 is required for the SRRC-based ODFBs with a roll-off coefficient of 0.1. When different roll-off coefficients are considered for the SRRC-based ODFBs, the EGF-based orthogonal digital filter induced aggregated upstream signal transmission capacity improvement ratios are calculated and presented in Fig. 14(c). In obtaining Fig. 14(c), the digital filter length of the proposed ODFBs is fixed at L=8, while the digital filter lengths of L=8 and L=16 are used for the SRRC-based ODFBs. The results indicate that for supporting an aggregated upstream signal transmission capacity similar to the proposed ODFBs with a digital filter length of L=8, the SRRC-based ODFBs must use a digital filter length of L≥32, which can, however, result in a 4× increase in the digital filter DSP complexity.

V. Differential ONU Optical Launch Power Dynamic Range

For the EGF-based and SRRC-based ODFBs, the considered four-ONU hybrid SSB OFDM-DFMA PON upstream performance robustness against differential ONU launch power variations [16] is explored, and the results are shown in Fig. 15, where the digital filter lengths of L=8 and L=16 are considered. Here the system setup illustrated in Section III(A) is utilized. The optimum digital filter parameter set of {α=0.23, ν=0.9, τ=1} is used to produce the required EGF-based ODFBs. A roll-off coefficient of 0.1 is utilized to generate the SRRC-based ODFBs. The SSMF transmission distance is 30km. The DAC/ADC resolution bits are taken to be 8. In the OLT, the received optical power is fixed at -2dBm.

It can be seen in Fig. 15 that for a digital filter length as short as L=8, the EGF-based ODFBs introduce >2.5dB improvements in the differential ONU launch power dynamic ranges compared to the SRRC-based ODFBs. Similar differential ONU launch power dynamic ranges can just be achieved for the EGF-based ODFBs with digital filter lengths of L=8 and L=16. In comparison with the EGF-based ODFBs with a digital filter length of L=8, the SRRC-based ODFBs with a digital filter length of L=16 only introduce <1.5dB improvements in the differential ONU launch power dynamic ranges. This implies that the proposed ODFBs can reduce the digital filter DSP complexity without greatly compromising the differential ONU launch power dynamic ranges.

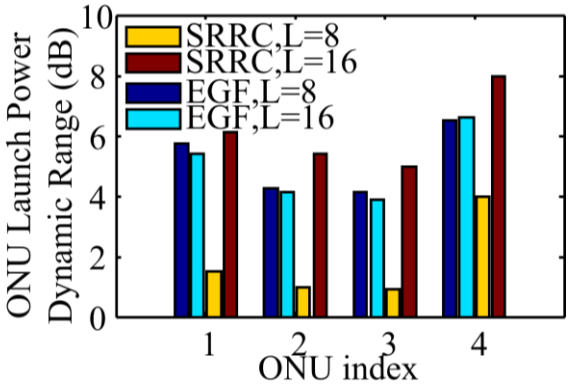

Fig. 15 Differential ONU launch power dynamic ranges.

VI. ONU Symbol Timing Offset

For the upstream transmissions of the hybrid OFDM-DFMA PONs, a FFT operation-based DSP operation is used in the OLT to simultaneously demultiplex and demodulate all the received SSB OFDM signals from different ONUs without utilizing digital matching filters. Such FFT-based signal demodulations, similar to the orthogonal frequency-division multiple access (OFDMA) based upstream transmission systems [34], [35], require synchronised symbol timing in all channels, otherwise large channel interferences may occur. In the upstream experimental demonstrations of the hybrid OFDM-DFMA PONs utilizing the SRRC-based ODFBs [15], [16], a digital domain time delay operation is conducted by adjusting the ONU symbol timing offset.

In this section, by utilizing the system setup and the parameters used in computing Fig. 15, the hybrid OFDM-DFMA PON upstream performance robustness against ONU symbol timing offset is explored and presented in Fig. 16. The ONU timing offset tolerance is defined as the maximum allowable timing offset from a specific ONU, over which all ONU BERs are less than the FEC limit at a fixed received optical power. In Fig. 16(a), the ONU timing offset tolerance of each ONU is normalized and presented as a percentage of the OFDM symbol time period (Ts). We can see that for the EGF-based ODFBs, similar ONU symbol timing offset tolerances are observed for the digital filter lengths of L=8 and L=16. While for the SRRC-based ODFBs, increasing the digital filter length from L=8 to L=16 improves each ONU's tolerance to symbol timing offset. For a digital filter length of L=8, the EGF-based ODFBs have relatively better performance robustness against ONU symbol timing offset compared to the SRRC-based ODFBs. We can also find that 30km SSMF transmissions do not greatly degrade the ONU symbol timing offset tolerances in comparison with the B2B transmissions. On the other hand, for the EGF-based ODFBs with a digital filter length of L=8, the tolerable symbol timing offsets are ~6.5% of the OFDM symbol time period, which are almost equal to the CP ratio of 1/16. Because the receiver DSP operation of the considered PON utilizes the FFT operation to demultiplex all the channels without incorporating any matching filters, therefore, similar to OFDMA PONs [34], the maximum ONU symbol timing offset range of the considered PON is determined by the CP ratio, this implies that for a digital filter length of L=8, the proposed ODFBs gives an ONU symbol timing offset tolerance equal to the CP-determined maximum ONU symbol timing offset range.

In Fig. 16(b), the impacts of the ONU-2 symbol timing offset on all other channels' BER performances are presented. Because the ONU-2 symbol timing offset exceeds the applied CP, the channel interference effect occurs. It can be found that if the symbol timing offset from a specific ONU is an integer multiple of the OFDM symbol time period, all other ONUs' transmission performances are not significantly degraded. Otherwise, the two channels in the vicinity of this ONU suffer from relatively large performance degradations. Therefore, these two channels present a periodic sudden drop in BERs when increasing the ONU timing offset. In addition, except

these two channels, all other channels, show relatively small performance degradations due to the digital filtering-induced channel interference reductions. As seen in Fig. 16(b), due to the ONU-2 (occupying CH3 and CH4) timing offsets, a considerable performance degradation is found for CH2 and CH5, while CH1 and CH8 have relatively small performance variations. This implies that due to the utilization of digital filtering in the ONU transmitters, the symbol timing offset from a specific ONU can degrade the transmission performances of the ONUs occupying adjacent channels only.

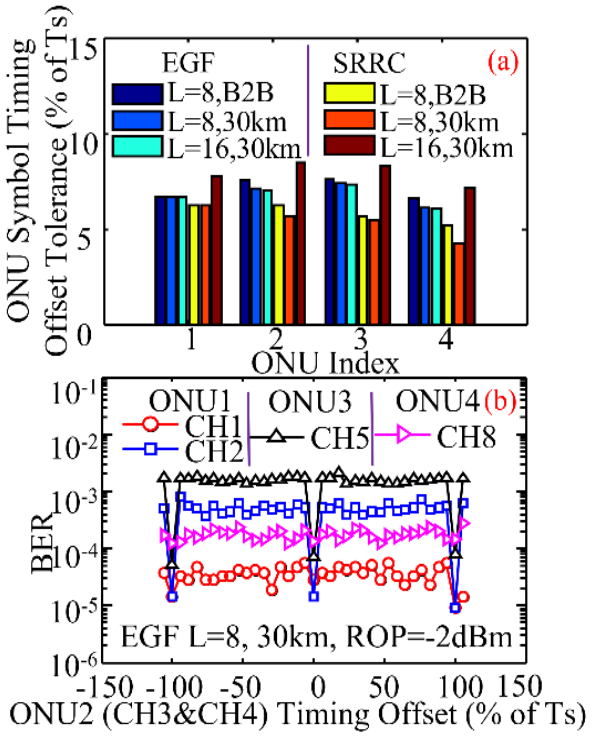

Fig. 16 (a) ONU symbol timing offset tolerance for each ONU and (b) impacts of ONU-2 symbol timing offset on BER performances of other channels.

VII. ONU Frequency Offset

For any ODFB-based multi-channel transmission systems, an ONU frequency offset may also introduce undesirable channel interferences. By utilizing the system setup and the parameters adopted in obtaining Fig. 15, ONU frequency offset tolerances are explored and shown in Fig. 17, where the received optical power of -2dBm is considered. In this figure, the ONU frequency offset tolerance is presented as a product of the OFDM symbol time period (Ts) and the maximum allowable frequency offset (Δf) associated with a specific ONU for a fixed received optical power. When ONU frequency offsets are less than Δf, all ONUs can have BERs below the FEC limit. In the considered PONs, for a specific ONU, the frequency offsets may occur after the DACs. In the OLT, a digital domain OFDM frequency offset correction technique [36] is utilized for estimating and compensating for the frequency offsets. In addition, 4 evenly distributed pilot subcarriers are also used in each channel to correct the residual frequency offsets [37].

The results in Fig. 17 show that for the EGF-based ODFBs, the digital filter lengths of L=8 and L=16 have similar performance robustness against the ONU frequency offset. While for the ONUs incorporating the SRRC-based ODFBs, increasing the digital filter length from L=8 to L=16 greatly improves their frequency offset tolerances. For a digital filter length of L=8 and 30km SSMF (B2B) transmissions, the EGF-based ODFBs improve the ONU frequency offset tolerances by a factor of >1.7 (>1.5) in comparison with the SRRC-based ODFBs. In addition, it can also be seen that for the ONUs suffering from the strong channel fading effect, the channel fading effect weakens their tolerances to the frequency offset.

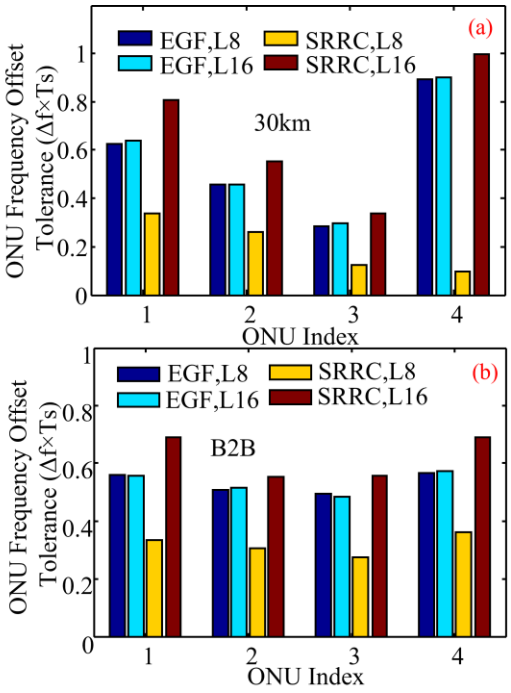

Fig. 17 ONU frequency offset tolerance for (a) 30km SSMF transmissions and (b) B2B transmissions.

The FFT-based frequency domain overlap-add method and the conventional convolution-based time domain method can be used for realizing the digital filtering operation. However, for transmission systems [10]-[12] similar to the PONs considered in this paper, before the digital filtering operation, a digital M× up-sampling operation should be performed via inserting (M-1) zeros between every two consecutive data samples. To support a large number of channel count, a large digital up-sampling factor of M is thus required. Therefore, when the total channel count is large, the considerable growth in digital filter DSP complexity is expected for both the FFT-based frequency domain digital filtering operation and the conventional convolution-based time domain digital filtering operation. To effectively solve the challenge, use can be made of a time domain digital filtering operation based on parallel digital filter DSP architectures. The corresponding real time implementation has been reported in [38], where the multiplication operations are not implemented for the zero-valued samples produced by the digital up-sampling operations. For such a time domain digital filtering process, a short digital filter can directly result in significant reductions in the digital filter DSP complexity [39].

For a specific PON suffering from the backscattering effects, the proposed EGF-based ODFBs can always outperform the SRRC-based ODFBs for a digital filter length of L=8, because of the larger stopband attenuations of the proposed ODFBs.

VIII. Conclusions

In this paper, a rectangular ODFB based on EGF has been proposed for realizing the orthogonal digital filtering-enabled multi-channel aggregation. The optimum digital filter parameters of the proposed ODFBs have been identified in upstream hybrid SSB OFDM-DFMA PONs based on IMDD. With the identified optimum digital filter parameters, for digital filter lengths of L=8 and L=16, the EGF-based ODFBs have ~6.4dB and ~12.6dB increases in the stopband attenuations compared to the previous SRRC-based ODFBs. In the passband of the proposed ODFBs with a digital filter length of L=8 (L≥16), the passband ripples are ~1.3dB (~2.3dB), which are mainly located at the central frequencies. For digital filter lengths of L≥32, the proposed ODFB's digital filter frequency responses are independent of digital filter length.

For the considered IMDD hybrid SSB OFDM-DFMA PONs, comprehensive upstream transmission performance comparisons have been made between the EGF-based ODFBs and the SRRC-based ODFBs. It has been shown that for the EGF-based ODFBs, increasing the digital filter length from L=8 to L=256 does not give rise to considerable improvements in neither the upstream PON transmission performances nor the maximum achievable aggregated upstream signal transmission capacities.

When use is made of the identified optimum digital filter length of L=8, in comparison with the SRRC-based ODFBs, the EGF-based ODFBs have the following unique advantages: 1) Improving the upstream receiver sensitivity by >1.5dB (>0.8dB) for 5-bit (8-bit) DAC/ADC resolutions, 2) Increasing the aggregated upstream signal transmission capacity by >5.5%. To achieve the same upstream signal transmission capacity, the SRRC-based ODFBs must prolong their digital filter lengths to L≥32. 3) Enlarging the differential ONU launch power dynamic ranges by >2.5dB, 4) Enhancing the ONU frequency offset tolerances by a factor of >1.5, and finally 5) Allowing a better tolerance to the ONU symbol timing offset. The work shows that the proposed ODFBs may offer a promising solution for constructing digital filter banks to realise flexible and elastic multi-channel aggregations with reduced digital filter DSP complexity.

For 5G and beyond application scenarios, the EGF-based rectangular prototype filters applied in the proposed rectangular ODFBs can be used to produce the rectangular digital filter banks required by filtered-OFDM. However, detailed theoretical and experimental explorations of their practically achievable performances and associated advantages for 5G networks are out of the scope of the present paper, which will be conducted in our research labs in due course.

References

[1] J. Zhang, Q. Liu, M. Zhu, H. Lin, S. Hu, X. Yi, and K. Qiu, "EML-based 200-Gbit/s/λ DMT signal transmission over 10-km SSMF using entropy loading and simplified volterra equalization," *Opt. Fiber Commun. Conf.*, W6A.32, USA, 2021.

[2] N. Stojanovic, F. Karinou, Z. Qiang, and C. Prodaniuc, "Volterra and wiener equalizers for short-reach 100G PAM-4 applications," *J. Light. Technol.*, vol. 35, no. 21, pp. 4583-4594, 2017.

[3] X. Li, Z. Xing, M. S. Alam, M. Jacques, and D. V. Plant, "102 Gbaud PAM-4 transmission over 2 km using a pulse shaping filter with asymmetric ISI and Thomlinson-Harashima Precoding," *Opt. Fiber Commun. Conf.*, T3I.1, USA, 2020.

[4] J. Zhang, J. Yu, K. Wang, W. Zhou, X. Xiao, J. Xiao, L. Zhao, X. Pan, B. Liu, and X. Xin, "200-Gb/s/λ PDM-PAM-4 PON with 29-dB power budget based on heterodyne coherent detection," *Opt. Fiber Commun. Conf.*, Th3F.1, USA, 2019.

[5] J. L. Wei, Q. Cheng, D. G. Cunningham, R. V. Penty, and I. H. White, "100-Gb/s hybrid multiband CAP/QAM signal transmission over a single wavelength," *J. Light. Technol.*, vol. 33, no. 2, pp. 415-423, 2015.

[6] X. Gao , Y. Cai , B. Xu , F. K. Deynu, and K. Qiu, "Zero guard band multi-twin-SSB system in single fiber bidirectional PON transmission," *IEEE Access*, vol. 8, pp. 26814-26826, 2020.

[7] ETSI, "Fifth generation fixed network (F5G), F5G 003 V1.11 (2021-09)", Sophia Antipolis, France, 2021.

[8] I. B. F. de Almeida, L. L. Mendes, J. J. P. C. Rodrigues, and M. A. A. da Cruz, "5G waveforms for IoT applications," *IEEE Commun. Surveys Tuts.*, vol. 21, no. 3, pp. 2554-2567, 3rd Quart., 2019.

[9] 3GPP, "Study on New Radio (NR) access technology V16.0.0 (2020-07)," Sophia Antipolis, France, TR 38.912.

[10] M. L. Deng, Q. W. Zhang, X. J. Guo, A. D. Wang, B. Lu, and L. Zhu, "Bandwidth-efficient and low-complexity mobile fronthaul utilizing digital orthogonal filtering-enabled channel aggregation," *Proc. Asia Commun. and Photon.*, Chengdu China, T4G.6, 2019.

[11] M. L. Deng, T. Mamadou, Z. B. Xing, X. Kang, Z. R. Luo, J. W. Shi, and L. Wang, "Digital orthogonal filtering-enabled synchronous transmissions of I/Q waveforms and control words for bandwidth-efficient and low-complexity mobile fronthaul," *Opt. Fiber Commun. Conf.*, F1D.2, USA, 2021.

[12] M. L. Deng, A. Sankoh, R. P. Giddings, and J. M. Tang, "Experimental demonstrations of 30Gb/s/λ digital orthogonal filtering-multiplexed multiple channel transmissions over IMDD PON systems utilizing 10G-class optical devices," *Opt. Express*, vol. 25, no. 20, pp. 24251-24261, 2017.

[13] S. Sarmiento, J. M. D. Mendinueta, J. A. Altabás, S. Spadaro, S. Shinada, H. Furukawa, J. J. V. Olmos, J. A. Lázaro, and N. Wada, "High capacity converged passive optical network and RoF-based 5G+ fronthaul using 4-PAM and NOMA-CAP signals," *J. Light. Technol.*, vol. 39, no. 2, pp. 372-380, 2021.

[14] W. Jin, A. Sankoh, Y. X. Dong, Z. Q. Zhong, R. P. Giddings, M. O'Sullivan, J. Lee, T. Durrant, and J. M. Tang, "Hybrid SSB OFDM-digital filter multiple access PONs," *J. Light. Technol.*, vol. 38, no. 8, pp. 2095-2105, 2020.

[15] Z. Zhong, W. Jin, S. Jiang, J. He, D. Chang, R. Giddings, Y. Hong, M. O'Sullivan, T. Durrant, G. Mariani, J. Trewern, and J. Tang, "Experimental demonstrations of concurrent adaptive inter-ONU and upstream communications in IMDD hybrid SSB OFDM-DFMA PONs," *Opt. Fiber Commun. Conf.*, F4I.5, USA, 2021.

[16] Z. Q. Zhong, W. Jin, S. Jiang, J. X. He, D. Chang, Y. H. Hong, R. P. Giddings, X. Q. Jin, M. O'Sullivan, T. Durrant, J. Trewern, G. Mariani, and J. M. Tang, "Concurrent inter-ONU communications for next generation mobile fronthauls based on IMDD hybrid SSB OFDM-DFMA PONs," *J. Light. Technol*, vol. 39, no. 23, pp. 7360-7369, 2021.

[17] M. Bolea, R. P. Giddings, M. Bouich, C. Aupetit-Berthelemot, and J. M. Tang, "Digital filter multiple access PONs with DSP-enabled software reconfigurability," *J. Opt. Commun. Netw.*, vol. 7, no. 4, pp. 215-222, 2015.

[18] M. Barrio, D. Izquierdo, J. A. Altabás, and I. Garcés, "50 Gb/s transmission using OSSB-MultiCAP modulation and a polarization independent coherent receiver for next-generation passive optical access networks," *J. Light. Technol*, ., vol. 39, no. 18, pp. 5722-5729, 2021.

[19] J. Estaran, M. I. Olmedo, D. Zibar, X. Xu, and I. T. Monroy, "First experimental demonstration of coherent CAP for 300-Gb/s metropolitan optical networks," *Opt. Fiber Commun. Conf.*, Th3K.3, USA, 2014.

[20] K. Z. Chen, L. W. Chen, C. Y. Lin, W. J. Huang, C. C. Wei, and J. Chen, "224-Gbps transmission for next-generation WDM long-reach PON using CAP modulation," *Opt. Fiber Commun. Conf.*, Tu2C.2, USA, 2016.

[21] Y. Zeng, Z. Dong, Y. Chen, X. Wu, H. He, J. You, and Q. Xiao, "A novel CAP-WDM-PON employing multi-band DFT-spread DMT signals based

on optical Hilbert-transformed SSB modulation," *IEEE Access*, vol. 7, pp. 29397-29404, 2019.

[22] M. Barrio, D. Izquierdo , J. Cerdá, S. Sarmiento, J. A. Altabás, J. A. Lázaro, and I. Garcés, "Spectrally efficient downstream 100 Gb/s PolMux Multi-CAP OSSB transmission and coherent reception Using 10G Electronics for passive optical networks," *Opt. Fiber Commun. Conf.*, F2H.3, USA, 2021.

[23] M. Xu, J. H. Yan, J. Zhang, F. Lu, J. Wang, L. Cheng, D. Guidotti, and G. K. Chang, "Bidirectional fiber-wireless access technology for 5G mobile spectral aggregation and cell densification," *J. Opt. Commun. Netw.*, vol. 8, no. 12, pp. B104-B110, 2016.

[24] P. Siohan and C. Roche, "Cosine-modulated filterbanks based on extended gaussian functions," *IEEE Trans. Signal Processing*, vol. 48, no. 11, pp. 3052-3061, 2000.

[25] Z. Q. Zhong, W. Jin, Y. X. Dong, A. Sankoh, J. X. He, Y. H. Hong, R. P. Giddings, I. Pierce, M. O'sullivan, J. Lee, G. Mariani, T. Durrant, and J. M. Tang, "Experimental demonstrations of matching filter-free digital filter multiplexed SSB OFDM IMDD transmission systems," *IEEE Photon. J.*, vol. 13, no. 2, pp. 7900512, 2021.

[26] W. Jin, Z. Q. Zhong, J. X. He, A. Sankoh, R. P. Giddings, Y. H. Hong, I. Pierce, M. O'Sullivan, C. Laperle, J. Lee, G. Mariani, T. Durrant, and J. M. Tang, "Experimental demonstrations of hybrid OFDM-digital filter multiple access PONs," *IEEE Photon. Technol. Lett.*, vol. 32, no. 13, pp. 751–754, 2020.

[27] A. Sahin, I. Guvenc, and H. Arslan, "A survey on multicarrier communications: Prototype filters, lattice structures, and implementation aspects," *IEEE Commun. Surveys Tuts.*, vol. 16, no. 3, pp. 1312-1338, 3rd Quart., 2014.

[28] X. Fang, Y. Fu, Q. Wu, L. Zhang, and F. Zhang, "Volterra expansion based intra channel nonlinear effect equalization method for optical OFDM/OQAM systems," *IEEE Access*, vol. 8, pp. 205657-205668, 2020.

[29] J. Nadal, C. A. Nour and A. Baghdadi, "Design and evaluation of a novel short prototype filter for FBMC/OQAM modulation," *IEEE Access*, vol. 6, pp. 19610-19625, 2018.

[30] M. Xu, J. Zhang, F. Lu, J. Wang, L. Cheng, M. I. Khalil, D. Guidotti, and G.-K. Chang, "Orthogonal multiband CAP modulation based on offset-QAM and advanced filter design in spectral efficient MMW RoF systems," *J. Light. Technol.*, vol. 35, no. 4, pp. 997-1005, 2016

[31] P. Guan, D. Wu, T. Tian, J. Zhou, X. Zhang, L. Gu, A. Benjebbour, M. Iwabuchi, and Y. Kishiyama, "5G field trials: OFDM-based waveforms and mixed numerologies," *IEEE J. Sel. Areas Commun.*, vol. 35, no. 6, pp. 1234-1243, Jun. 2017.

[32] J. Mao, L. Zhang, P. Xiao, and K. Nikitopoulos, "Filtered OFDM: an insight into intrinsic in-band interference and filter frequency response selectivity," *IEEE Access*, vol. 8, pp. 100670-100683, 2020.

[33] X. Fang, Y. Wang, Z. Suo, H. Jiang, X. Gao, L. Zhang, and D. Ding, "Analysis of the time-frequency localization property of the filter banks for optical OFDM/OQAM systems," *J. Light. Technol*, vol. 37, no. 21, pp. 5392-5405, 2019.

[34] S. Y. Jung, S. M. Jung, H. J. Park, and S. K. Han, "Mitigation of timing offset effect in IM/DD based OFDMA-PON uplink multiple access," *Opt. Express*, vol. 23, no. 11, pp. 13889-13898, 2015.

[35] A. Aminjavaheri, A. Farhang, A. RezazadehReyhani, and B. Farhang-Boroujeny, "Impact of timing and frequency offsets on multicarrier waveform candidates for 5G," *Proc. IEEE Signal Process. Signal Process. Edu. Workshop*, pp. 178–183, 2015.

[36] P. H. Moose, "A technique for orthogonal frequency division multiplexing frequency offset correction," *IEEE Trans. Commun.*, vol. 42, no. 10, pp. 2908-2914, 1994.

[37] X. Yi, W. Shieh, and Y. Tang, "Phase estimation for coherent optical OFDM," *IEEE Photon. Technol. Lett.*, vol. 19, no. 12, pp. 919–921, 2007.

[38] E. Al-Rawachy, R. P. Giddings, and J. Tang, "Experimental demonstration of a real-time digital filter multiple access PON with low complexity DSP-based interference cancellation," *J. Light. Technol.*, vol. 37, no. 17, pp. 4315-4329, 2019.

[39] J. L. Wei, C. Sanchez, and E. Giacoumidis, "Fair comparison of complexity between a multiband CAP and DMT for data center interconnects," *Opt. Lett.*, vol. 42, no. 19, pp. 3860-3863, 2017.